J Mol Model (2010) 16:577–587
DOI 10.1007/s00894-009-0574-2

ORIGINAL PAPER

Experimental and quantum chemical calculational studies on 2-[(4-Fluorophenylimino)methyl]-3,5-dimethoxyphenol

Hasan Tanak · Ayşen Ağar · Metin Yavuz

Received: 12 May 2009 / Accepted: 26 July 2009 / Published online: 25 August 2009

Abstract The Schiff base compound, 2-[(4-Fluorophenylimino)methyl]-3,5-dimethoxyphenol, has been synthesized and characterized by IR, electronic spectroscopy, and X-ray single-crystal determination. Molecular geometry from X-ray experiment of the title compound in the ground state have been compared using the Hartree-Fock (HF) and density functional method (B3LYP) with 6–31G(d) basis set. Calculated results show that density functional theory (DFT) and HF can well reproduce the structure of the title compound. The energetic behavior of the title compound in solvent media has been examined using B3LYP method with the 6–31G(d) basis set by applying the polarizable continuum model (PCM). The total energy of the title compound decrease with the increasing polarity of the solvent. By using TD-DFT and TD-HF methods, electronic absorption spectra of the title compound have been predicted and a good agreement with the TD-DFT method and the experimental ones is determined. In addition, DFT calculations of the title compound, molecular electrostatic potential (MEP), natural bond orbital (NBO), and thermodynamic properties were performed at B3LYP/6–31G(d) level of theory.

H. Tanak (✉) · M. Yavuz
Department of Physics, Faculty of Arts and Sciences,
Ondokuz Mayis University,
55139, Kurupelit,
Samsun, Turkey
e-mail: htanak@omu.edu.tr

A. Ağar
Department of Chemistry, Faculty of Arts and Sciences,
Ondokuz Mayis University,
55139, Kurupelit,
Samsun, Turkey

Keywords Density functional theory · Electronic absorption spectra · Hartree-Fock · Molecular electrostatic potential · Schiff base · Vibrational assignment

Introduction

Schiff bases, *i.e.*, compounds having a double C=N bond, are used as starting materials in the synthesis of important drugs, such as antibiotics and antiallergic, antiphlogistic, and antitumor substances [1–3]. On the industrial scale, they have a wide range of applications, such as dyes and pigments [4]. They are also used as components of rubber compounds [5]. Schiff base compounds display interesting photochromic and thermochromic features in the solid state and can be classified in terms of these properties [6]. Photo- and thermochromism arise *via* H-atom transfer from the hydroxy O atom to the imine N atom [7, 8]. Such proton-exchanging materials can be utilized for the design of various molecular electronic devices [9]. In general, Schiff bases display two possible tautomeric forms, the phenol-imine (OH) and the keto-amine (NH) forms. Depending on the tautomers, two types of intramolecular hydrogen bonds are observed in Schiff bases: O-H···N in phenol-imine [10–14] and N-H···O in keto-amine [15–17] tautomers.

By means of increasing development of computational chemistry in the past decade, the research of theoretical modeling of drug design, functional material design, *etc*., has become more mature than ever. Many important chemical and physical properties of biological and chemical systems can be predicted from the first principles by various computational techniques [18]. In recent years, density functional theory (DFT) has been a shooting star in theoretical modeling. The development of better and better

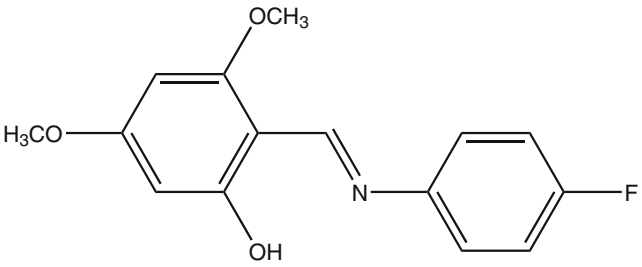

Fig. 1 Chemical diagram of the title compound $C_{15}H_{14}FNO_3$

exchange-correlation functionals made it possible to calculate many molecular properties with comparable accuracies to traditional correlated *ab initio* methods, with more favorable computational costs [19]. Literature survey revealed that the DFT has a great accuracy in reproducing the experimental values of geometry, dipol moment, vibrational frequency, *etc*. [20–26].

In this paper, we wish to report the synthesis, characterization and crystal structure of the Schiff base, 2-[(4-Fluorophenylimino)methyl]-3,5-dimethoxyphenol (Fig. 1), as well as the theoretical studies on it by using HF/6-31G (d) and DFT/B3LYP/6-31G(d) methods. The properties of the structural geometry, molecular electrostatic potential (MEP), natural bond orbital analysis (NBO) and the thermodynamic properties for the title compound at the B3LYP/6-31G(d) level were studied. We also make comparisons between experiments and calculations.

Experimental

The compound 2-[(4-Fluorophenylimino)methyl]-3,5-dimethoxyphenol was prepared by reflux a mixture of a solution containing 2-Hydroxy-4,6-dimethoxy-benzaldehyde (0.0431 g 0.237 mmol) in 20 ml ethanol and a solution containing 2,4-Dimethylaniline (0.0263 g 0.237 mmol) in 20 ml ethanol. The reaction mixture was stirred for 1 hundred reflux. The crystals of 2-[(4-Fluorophenylimino) methyl]-3,5-dimethoxyphenol suitable for X-ray analysis were obtained from ethylalcohol by slow evaporation (yield %51; m.p.380–382 K). The IR spectra were recorded in the 4000–400 cm^{-1} region using KBr pellets on a Schmadzu FTIR-8900 spectrophotometer. Electronic absorption spectra were measured on a Unicam UV-VIS spectrophotometer in ethanol.

Crystal data for the title compound

CCDC 730021, $C_{15}H_{14}FNO_3$, Mw=275.27, monoclinic, space group *C*2/*c*; Z=8, a=22.654(11) Å, b=10.928(6) Å, c=12.014(6) Å, β=114.082(4)° and V=2715(2) $Å^3$ F(000)= 1151.8, Dx=1.346 g/cm^3.

Computational methods

The molecular geometry is directly taken from the X-ray diffraction experimental result without any constraints. In the next step, the DFT calculations with a hybrid functional B3LYP (Becke's three parameter hybrid functional using the LYP correlation functional) at 6–31G(d) basis set and the Hartree-Fock calculations at 6–31G(d) basis set by the Berny method [27, 28] were performed with the Gaussian 03 software package [29]. The harmonic vibrational frequencies were calculated at the same level of theory for the optimized structures and the obtained frequencies were scaled by 0.9627 and 0.8929 [30], respectively. By using Gauss-View molecular visualization program [31], the vibrational bands assignments have been made. In order to evaluate the energetic and dipole moments behavior of the title compound in solvent media, we carried out optimization calculations in the three kinds of solvent (chloroform, ethanol, and water) by using polarizable continuum model (PCM) theory [32–35]. The electronic absorption spectra was calculated using the time-dependent density functional theory (TD-DFT) and

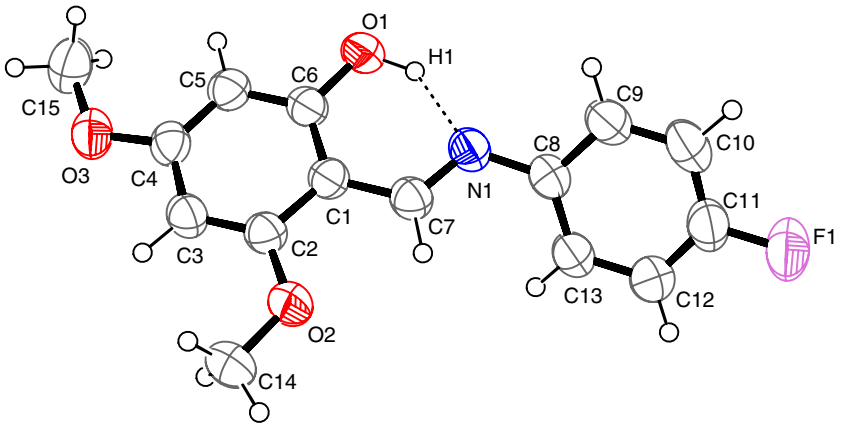

Fig. 2 Ortep 3 diagram of the title compound. Displacement ellipsoids are drawn at the 50% probability level and H atoms are shown as small spheres of arbitrary radii

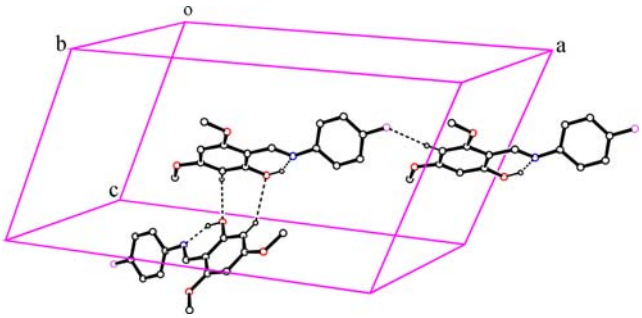

Fig. 3 Part of the crystal structure of the title compound showing the intra- and inter molecular interactions as dashed lines. H atoms not involved in hydrogen bonding have been omitted for clarity

Hartree-Fock (TD-HF) methods [36–39]. In addition, the electronic absorption spectra was calculated in ethanol solution with the PCM method. To investigate the reactive sites of the title compound the molecular electrostatic potential were evaluated using B3LYP/6–31G(d) method. Molecular electrostatic potential, $V(r)$, at a given point $r(x,y,z)$ in the vicinity of a molecule, is defined in terms of the interaction energy between the electrical charge generated from the molecule's electrons and nuclei and a positive test charge (a proton) located at r. For the system studied the $V(r)$ values were calculated as described previously using the equation [40],

$$V(r) = \sum Z_A \Big/ |R_A - r| - \int \rho(r') \Big/ |r' - r| \, d^3r' \qquad (1)$$

where Z_A is the charge of nucleus A, located at R_A, $\rho(r')$ is the electronic density function of the molecule, and r' is the dummy integration variable. The thermodynamic properties of the title compound at different temperatures were calculated on the basis of vibrational analyses.

Results and discussion

Crystal structure

In the title compound, the molecular structure is not planar. The dihedral angle between the aromatic ring systems is 42.45(5)°. It is also known that Schiff bases may exhibit thermochromism depending on the planarity or non-planarity, respectively [41]. The phenol H atom form a strong intramolecular hydrogen bond with the imine N atom, it is consistent with the related structure [12].

The length of the C=N double bond is 1.287(2)Å, and is consistent with the standard 1.28Å value of C=N double bond. The imino group is coplanar with the hydroxyphenyl ring as can be shown by the C6-C1-C7-N1 torsion angle of 3.6(2)°.

The molecular structure is stabilized by intra and intermolecular hydrogen bonds. An intramolecular O1-H1···N1 hydrogen bond generates a six-membered ring (Fig. 2), producing an S(6) ring motif [42], resulting in approximate planarity of the molecular skeleton [O···N=2.612(2)Å]. In the crystal structure, molecules are linked together by intermolecular C-H···O and C-H···F interactions (Fig. 3), namely C3-H3···F1 (symmetry code: x-1/2, y-1/2, z) and C5-H5···O1 (symmetry code: −x, y, −z+1/2). The crystal structure is further stabilized by intermolecular C-H···π stacking interaction [C15-H15B···Cg(2) with symmetry code: −x, −y, 1−z , Cg(2) ring is consistent with C8/C9/C10/C11/C12/C13], the details of the hydrogen bonds are shown in Table 1.

Optimized geometries

B3LYP/6–31G(d) and HF/6–31G(d) calculations were performed on the title compound, respectively. Calculated geometric parameters are listed in Table 2 along with the

Table 1 Hydrogen-bond geometry (Å, º)

D—H···A	D—H	H···A	D···A	D—H···A
X-ray				
C3–H3···F1^{i}	0.972(17)	2.522(18)	3.492(2)	176.5(13)
C5–H5···O1^{ii}	0.951(19)	2.592(19)	3.419(3)	145.5(14)
O1–H1···N1	0.82	1.88	2.6121(19)	148.3
C15–H15B···Cg(2)^{iii}	0.99(3)	2.69(2)	3.660(3)	166(2)
B3LYP/6–31G(d)				
C3–H3···F1^{i}	1.081	2.432	3.513	179.1
C5–H5···O1^{ii}	1.082	2.583	3.656	170.6
O1–H1···N1	1.004	1.699	2.609	148.4
HF/6–31G(d)				
C3–H3···F1^{i}	1.069	2.637	3.697	170.6
C5–H5···O1^{ii}	1.070	2.813	3.875	171.1
O1–H1···N1	0.962	1.838	2.677	144

Symmetry codes: (i) x−1/2, y−1/2, z (ii) −x, y, −z+1/2 (iii) −x, −y, 1−z

Table 2 Selected molecular structure parameters

Parameters	Experimental	Calculated 6–31G(d)	
		HF	B3LYP
Bond lengths (Å)			
O1–C6	1.3463(18)	1.324	1.338
C6–C5	1.385(2)	1.395	1.402
C6–C1	1.408(2)	1.401	1.423
C1–C2	1.416(2)	1.415	1.426
C1–C7	1.433(2)	1.457	1.440
O3–C4	1.3619(19)	1.336	1.358
O3–C15	1.418(3)	1.403	1.422
N1–C7	1.288(2)	1.267	1.298
N1–C8	1.410(2)	1.408	1.406
C5–C4	1.378(2)	1.377	1.391
C4–C3	1.397(2)	1.402	1.410
O2–C2	1.362(2)	1.342	1.362
O2–C14	1.417(2)	1.403	1.420
C2–C3	1.368(2)	1.373	1.384
C8–C13	1.388(2)	1.390	1.406
C8–C9	1.392(2)	1.392	1.405
C13–C12	1.372(3)	1.386	1.393
F1–C11	1.362(2)	1.332	1.351
C9–C10	1.374(3)	1.381	1.391
C11–C12	1.359(3)	1.375	1.389
C11–C10	1.364(3)	1.379	1.390
RMSE		0.015	0.014
Bond angles (°)			
O1-C6-C5	117.86(14)	116.38	117.57
O1-C6-C1	120.34(14)	122.11	121.24
C5-C6-C1	121.81(14)	121.49	121.18
C6-C1-C2	117.09(14)	117.54	117.69
C6-C1-C7	122.31(13)	122.39	121.49
C2-C1-C7	120.59(14)	120.05	120.81
C4-O3-C15	118.38(15)	120.06	118.46
C7-N1-C8	118.33(14)	120.11	121.00
C4-C5-C6	118.71(15)	118.97	119.09
N1-C7-C1	122.57(15)	123.10	122.08
O3-C4-C5	124.43(15)	124.00	124.12
O3-C4-C3	113.85(14)	114.64	114.42
C5-C4-C3	121.72(15)	121.35	121.44
C2-O2-C14	118.68(15)	120.24	118.62
O2-C2-C3	124.02(14)	123.08	123.47
O2-C2-C1	114.28(14)	115.34	115.15
C3-C2-C1	121.69(15)	121.56	121.37
C13-C8-C9	118.23(16)	118.77	118.65
C13-C8-N1	122.94(14)	123.10	123.49
C9-C8-N1	118.79(15)	118.07	117.81
C2-C3-C4	118.97(15)	119.07	119.21
C12-C13-C8	121.22(17)	120.74	120.74
C10-C9-C8	120.57(18)	120.92	121.00
C12-C11-F1	118.61(19)	119.17	119.10
C12-C11-C10	122.51(18)	121.75	121.75
F1-C11-C10	118.86(17)	119.06	119.13
C11-C10-C9	118.88(17)	118.83	118.82
C11-C12-C13	118.53(19)	118.93	118.98
RMSE		0.84	0.72
Torsion angles (°)			
O1-C6-C1-C2	178.88(13)	−179.88	−179.61
O1-C6-C1-C7	−2.4(2)	0.08	0.36
C8-N1-C7-C1	−175.81(14)	178.36	176.96
C15-O3-C4-C5	1.6(2)	−0.10	−0.14
C6-C5-C4-O3	−179.96(14)	−179.98	179.95
C14−O2-C2-C1	−179.00(17)	-179.54	−179.74
C6-C1-C2-O2	179.39(13)	−179.96	179.83
C7-N1-C8-C13	38.4(2)	−42.60	−33.55
C7-N1-C8-C9	−143.94(16)	139.73	148.67
N1-C8-C13-C12	−179.77(17)	−179.30	−179.39
F1-C11-C10-C9	179.87(17)	−179.63	−179.48
F1-C11-C12-C13	−179.89(18)	179.88	179.81

experimental data. When the X-ray structure of the title compound is compared with its optimized counterparts (see Fig. 4), conformational discrepancies are observed between them. The most remarkable discrepancies exist in the orientation of the flourophenyl ring in the title compound. The orientation of the flourophenyl ring is defined by torsion angles C1-C7-N1-C8 [−175.81(14)º] and C7-N1-C8-C9 [−143.94(16)°]. These torsion angles have been calculated at 178.36º and 139.73° for HF/6–31G(d) level, 176.96º and 148.67° for B3LYP/6–31G(d) level, respectively. The methoxy groups are almost coplanar with the attached ring with C15-O3-C4-C5 and C14-O2-C2-C1 torsion angles of 1.6(2)º and −179(17)º for X-ray while the corresponding values are calculated as −0.10º and −179.54º for HF, and −0.14º and −179.74º for B3LYP, respectively.

As seen from Table 2, the optimized bond lengths are slightly different than the experimental values. The biggest differences of bond lengths between the experimental and the predicted values are found at C11–C12 bond, with the different values being 0.031 Å for B3LYP method and F1–C11 bond with a value 0.029 Å for HF method. For the bond angles, the biggest differences occur at C7-N1-C8 bond angle, with the different values being 2.67º for B3LYP method and 1.78º for HF method. According to above comparisons, it can be deduced that, for the title compound, the biggest differences of bond lengths and

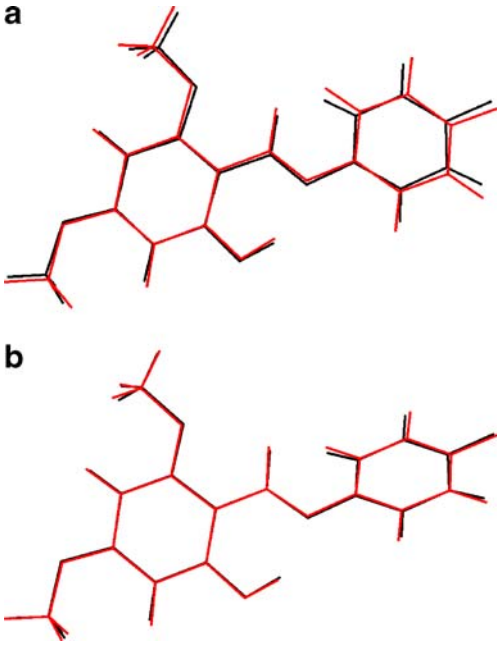

Fig. 4 Atom-by-atom superimposition of the structures calculated (red) (**a**=DFT ; **b**=HF) over the X-ray structure (black) for the title compound

bond angles mainly occur in the groups involved in the hydrogen bonds [*i.e.*, F1-C11 and C7-N1-C8], which can be easily understood taking into account the intra— and intermolecular hydrogen bond interactions present in the crystal.

In order to compare the theoretical results with the experimental values, root mean square error (RMSE) is used. Calculated RMSE for bond lengths and bond angles are 0.014 Å and 0.72º for B3LYP method, and 0.015 Å and 0.84º for HF method, respectively. A logical method for globally comparing the structures obtained with the theoretical calculations is by superimposing the molecular skeleton with that obtained from X-ray diffraction, giving a RMSE of 0.183 Å for B3LYP and 0.111 Å for method HF (Fig. 4). According to these results, it may be concluded that the B3LYP calculation well reproduce the bond lengths and angles of the title compound, while the HF method is better in predicting the 3-D geometry of the title compound. In spite of the some differences, calculated geometric parameters represent a good approximation and they are the bases for calculating other parameters, such as vibrational frequencies, electronic absorption spectra, molecular electrostatic potential and thermodynamic properties, as we described below.

IR spectroscopy

Harmonic vibrational frequencies of the title compound were calculated by using DFT/B3LYP and HF method with 6–31G(d) basis set. By using Gauss-View molecular visualization program, the vibrational bands assignments have been made. In order to facilitate assignment of the observed peaks we have analyzed some vibrational fre-

Table 3 Comparison of the experimental and calculated vibrational frequencies (cm^{-1})

Assignment [a]	Experiment	HF/6–31G(d)	B3LYP/6–31G(d)
ν (O-H)	3470.3	3383.1	2935.4
ν_{ring} (C-H)	3108.1	3063.2	3125.9
ν_{s} (CH_3)	2970.2	2977.7	3040.1
ν_{as} (CH_3)	2944.2	2940.7	2979.2
ν(C=N)	1608.7	1666.2	1610.6
ν(C=C)	1566.5	1576.5	1564.7
γ(OH) + ω(CH_3) + γ_{ring}(C-H)	1512.2	1515.9	1512.1
γ(OH) + ω(CH_3) + γ_{ring}(C-H)	1495.5	1500.7	1491.5
γ(OH) + α (CH_3)	1466.7	1481.6	1475.4
γ(OH) + ω(CH_3) + γ_{ring}(C-H)	1443.9	1453.2	1443.1
γ(CH) + γ(OH) + ω(CH_3)	1400.9	1389.1	1409.5
ν(C-O) + ω(CH_3) + γ(OH) + ν(C-C)	1345.7	1340.1	1342.7
ν(C-F) + γ(CH) + ν(C-C)	1221.3	1229.1	1227.4
ω(CH_3) + γ_{ring}(C-H) + ν(C-O)	1203.6	1220.3	1199.5
ω(CH_3) + ν(C-O) + γ_{ring}(C-H)	1152.6	1168.6	1153.2
γ_{ring}(C-H) + γ(C-H) + ω(CH_3) + ν(C-O)	1116.9	1125.7	1114.9
γ_{ring}(C-H)	1094.9	1058.3	1084.5
ω_{ring}(C-H)	826.8	844.1	827.3
δ_{ring}(C-H)	771.3	807.6	771.8

[a] ν, stretching; α, scissoring; γ , rocking; ω, wagging; δ, twisting; s, symmetric; as, asymmetric

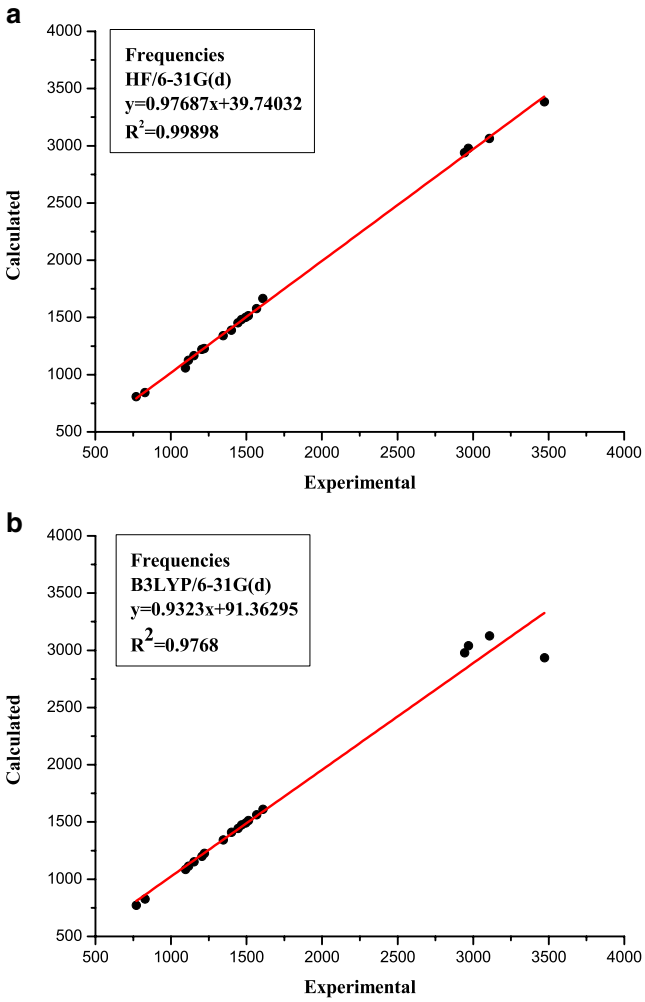

Fig. 5 Correlation graphics of calculated and experimental frequencies of the title compound

quencies and compared our calculation of the title compound with their experimental results as shown in Table 3.

The experimental O-H stretching mode was observed at 3470.3 cm^{-1}, which have been calculated with B3LYP and HF at 2935.4 and 3383.1 cm^{-1}, respectively. As can be easily seen the experimental value of O-H stretching mode is closer to HF value than that of B3LYP. The aromatic structure shows the presence of C-H stretching vibrations in the region 2900–3150 cm^{-1} which is the characteristic region for the ready identification of the C-H stretching vibrations. In this region, the bands are not affected, appreciably by the nature of the substituents [43]. The C-H aromatic stretching mode was observed to be 3108.1 cm^{-1} experimentally, while it has been calculated at 3125.9 cm^{-1} for B3LYP and 3063.2 cm^{-1} for HF, respectively. The bands at 2944.2 and 2970.2 cm^{-1} correspond to the asymmetric and symmetric stretching CH3 modes, respectively. These bands have been calculated at 2940.7 and 2977.7 cm^{-1} for HF, and 2979.2 and 3040.1 cm^{-1} for B3LYP, respectively.

The experimental C=C and C=N stretch bands were observed at 1566.5 and 1608.7 cm^{-1}, which have been calculated with HF and B3LYP at 1576.5–1666.2 and 1564.7–1610.6 cm^{-1}, respectively. The above conclusions are in good agreement with the literature values [44, 45]. The strong absorption band at 1221.3 cm^{-1} in the infrared experimental spectrum is due to the stretching vibration of C-F. This band has been calculated at 1229.1 cm^{-1} for HF level, and 1227.4 cm^{-1} for B3LYP level. The band is in good agreement with the literature value (1230 cm^{-1}) obtained for 2-fluoro-4,6-dinitrophenol [46]. The other calculated vibrational frequencies can be seen in Table 3.

To make a comparison with the experimental observation, we present correlation graphics in Fig. 5 based on the calculations. As we can see from correlation graphics in Fig. 5 experimental fundamentals are found to have a better correlation with HF than B3LYP. Besides, the vibrational frequencies calculated by B3LYP method are more compatible to experimental values with the exception of O-H stretching mode which has the correlation coefficient R^2= 0.99973.

Energetics and dipole moments

In order to evaluate the energetic behavior of the title compound in solvent media, we carried out calculations in three kinds of solvent (water, ethanol, chloroform). Total molecular energies, frontier molecular orbital energies and dipole moments have been calculated in solvent media with B3LYP/6-31G(d) level using PCM model and the results are presented in Table 4. According to Table 4, we can conclude that obtained total molecular energies and energy

Table 4 Calculated energies, dipole moments and frontier orbital energies

	Gas phase (ε=1)	Chloroform (ε=4.9)	Ethanol (ε=24.55)	Water (ε=78.39)
E_{TOTAL} (Hartree)	−960.26593882	−960.26948602	−960.27073125	−960.27104002
E_{HOMO} (eV)	−5.499	−5.608	−5.645	−5.651
E_{LUMO} (eV)	−1.385	−1.495	−1.536	−1.545
ΔE (eV)	4.114	4.113	4.109	4.106
μ (D)	3.816	4.322	4.469	4.512

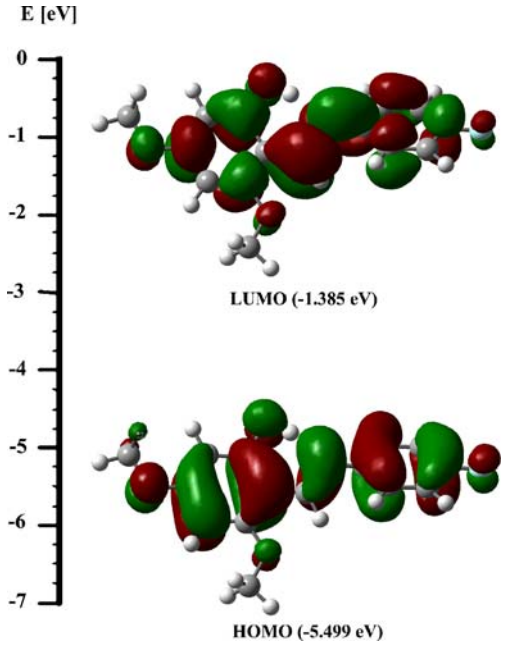

Fig. 6 HOMO and LUMO of the title compound

gap (ΔE) between the highest occupied molecular orbital (HOMO) and the lowest unoccupied molecular orbital (LUMO) of the title compound by PCM method decreases with the increasing polarity of the solvent and while the dipole moments will increase with the increase of the polarity of the solvent. Solvent effects improve the charge delocalized in the molecules, therefore, inducing the dipole moments to be raised. Ground-state dipole moment is an important factor in measuring solvent effect, a large ground-state dipole moment gives rise to strong solvent polarity effects [47, 48].

Electronic absorption spectra

The UV-visible spectrum of *ortho* hydroxylated Schiff bases which exist mainly as phenol-imine structure indicates the presence of a band at <400 nm, while compounds that exist as keto-amine form show a new band, especially in polar and nonpolar solvents at >400 nm [49–56]. Experimentally, electronic absorption spectra of the title compound in ethanol solvent show two bands at 332 and 499 nm, which correspond to phenol-imine and keto-amine forms, respectively. These values are similar to those found in related compounds [9, 57]. According to experimental results, the phenol-imine form is dominant in ethanol solvent which has absorption band at 332 nm with log ε=4.629.

Electronic absorption spectra were calculated by TD-DFT and TD-HF methods based on the B3LYP/6–31G(d) and HF/6–31G(d) levels optimized structure in gas phase, respectively. The predicted absorption wavelengths are at 244.16 nm with oscillator strength being 0.7792 for TD-HF and 329.65 nm with the oscillator strength being 0.6688 for TD-DFT calculations. It is obvious that to use TD-DFT calculations to predict the electronic absorption spectra is more reasonable than TD-HF method. In addition to the calculations in gas phase, TD-DFT calculations of the title compound in ethanol solvent were performed by using PCM model. The PCM calculation reveal that the calculated absorption band has red shift with a value 336.89 nm with oscillator strength being 0.887. The reason for this red shift is solvent effect which can effect the geometry and electronic structure as well as the properties of the molecule as solvent effects induce the lower energy of the molecules, and generate more significant red shift for absorption bands

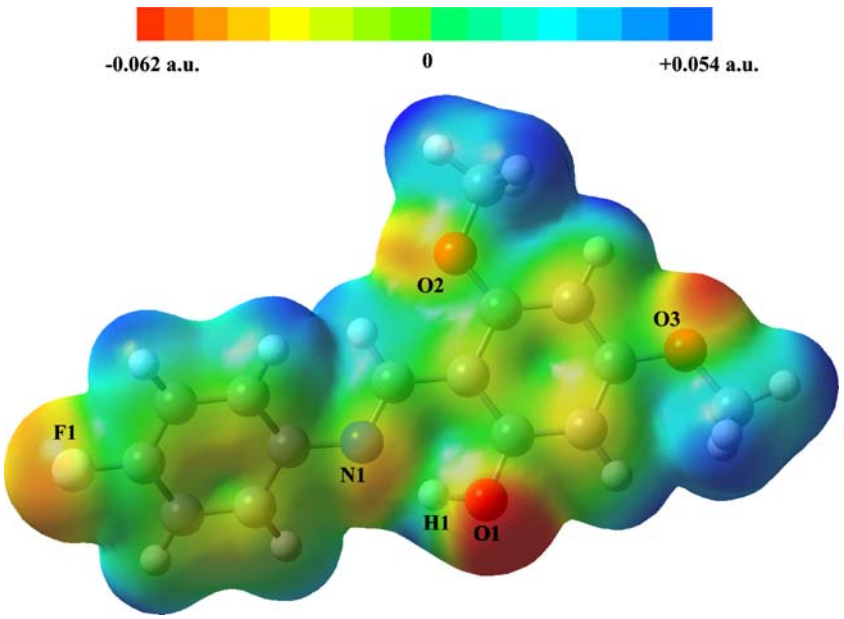

Fig. 7 Molecular electrostatic potential map calculated at B3LYP/6–31G(d) level

Table 5 Selected natural bond orbital occupancies of the title compound

NBO	Occupancies (a.u.)	NBO	Occupancies (a.u.)
BD(1) O1–C6	1.994	BD*(1) O1–C6	0.017
BD(1) C1–C6	1.973	BD*(1) C1–C6	0.033
BD(2) C1–C6	1.606	BD*(2) C1–C6	0.469
BD(1) C5–C6	1.973	BD*(1) C5–C6	0.022
BD(1) C1–C7	1.974	BD*(1) C1–C7	0.024
BD(1) C1–C2	1.967	BD*(1) C1–C2	0.026
BD(1) O3–C4	1.991	BD*(1) O3–C4	0.028
BD(1) O3–C15	1.992	BD*(1) O3–C15	0.008
BD(1) N1–C7	1.987	BD*(1) N1–C7	0.011
BD(2) N1–C7	1.912	BD*(2) N1–C7	0.236
BD(1) N1-C8	1.983	BD*(1) N1–C8	0.027
BD(1) C4–C5	1.978	BD*(1) C4–C5	0.025
BD(2) C4–C5	1.705	BD*(2) C4–C5	0.391
BD(1) C3–C4	1.969	BD*(1) C3–C4	0.021
BD(1) O2–C2	1.991	BD*(1) O2–C2	0.026
BD(1) O2–C14	1.992	BD*(1) O2–C14	0.008
BD(1) C2–C3	1.977	BD*(1) C2–C3	0.022
BD(2) C2–C3	1.745	BD*(2) C2–C3	0.369
BD(1) C8–C13	1.976	BD*(1) C8–C13	0.029
BD(2) C8–C13	1.639	BD*(2) C8–C13	0.392
BD(1) C8–C9	1.974	BD*(1) C8–C9	0.023
BD(1) C12–C13	1.973	BD*(1) C12–C13	0.013
BD(1) F1–C11	1.995	BD*(1) F1–C11	0.030
BD(1) C9–C10	1.973	BD*(1) C9–C10	0.012
BD(2) C9–C10	1.695	BD*(2) C9–C10	0.333
BD(1) C10–C11	1.982	BD*(1) C10–C11	0.027
BD(1) C11–C12	1.982	BD*(1) C11–C12	0.027
BD(2) C11–C12	1.658	BD*(2) C11–C12	0.384

Note. BD for 2-center bond and BD* for 2-center antibond, a serial number (1, 2, . . . if there is a single, double, . . . bond between the pair of atoms), and the atom(s) to which the NBO is affixed

[58]. For the title compound, TD-DFT method for both in gas phase and solvent media is convenient to predict the electronic absorption spectra.

According to the TD-DFT calculational electronic absorption spectra shows the maximum absorption wavelength corresponding to the electronic transition from the highest occupied molecular orbital (HOMO) to the lowest unoccupied molecular orbital (LUMO). The frontier molecular orbitals (HOMO and LUMO) of the title compound are shown in Fig. 6. As seen from Fig. 6, both the HOMO and LUMO are mainly localized on the whole structure except methyl groups. Molecular orbital coefficients analyses based on optimized geometry indicate that, for the title compound, the frontier molecular orbitals are

Table 6 Second-order perturbation theory analysis of the Fock matrix in NBO basis, calculated at B3LYP/6–31G(d) level

Donor orbital (*i*)	Acceptor orbital (*j*)	$E^{(2)}$ [c] (*kcal/mol*)	ε_j-ε_i [a] (*a.u.*)	F_{ij} [b] (*a.u.*)
LP(1) F1	BD*(1) C3-H3	0.48	1.51	0.024
LP(2) F1	BD*(1) C3-H3	1.02	0.91	0.027
LP(3) F1	BD*(1) C3-H3	0.46	0.90	0.018
LP (1) O1	BD*(1) C5- H5	1.39	1.05	0.034
LP (2) O1	BD*(1) C5- H5	0.10	0.80	0.009
LP (1) N1	BD*(1) H1-O1	34.83	0.76	0.148

[a] Energy difference between donor and acceptor *i* and *j* NBO orbitals

[b] F_{ij} is the Fock matrix element between *i* and *j* NBO orbitals

[c] $E^{(2)}$ means energy of hyper conjugative interactions

mainly composed of *p* atomic orbitals, so above electronic transitions are mainly derived from the contribution of bands $\pi \rightarrow \pi^*$.

Molecular electrostatic potential

Molecular electrostatic potential (MEP) is related to the electronic density and is a very useful descriptor in understanding sites for electrophilic attack and nucleophilic reactions as well as hydrogen bonding interactions [59, 60]. The electrostatic potential $V(r)$ is also well suited for analyzing processes based on the "recognition" of one molecule by another, as in drug-receptor, and enzyme-substrate interactions, because it is through their potentials that the two species first "see" each other [61, 62]. Being a real physical property $V(r)s$ can be determined experimentally by diffraction or by computational methods [63].

To predict reactive sites of electrophilic and nucleophilic attack for the investigated molecule, MEP at the B3LYP/6–31G(d) optimized geometry was calculated. The negative (red and yellow) regions of MEP were related to electrophilic reactivity and the positive (blue) regions to nucleophilic reactivity (Fig. 7). As can be seen in Fig. 7, there are several possible sites of electrophilic attack. Negative regions in the studied molecule were found around the phenol O1 atom, O2, and O3 atoms of the methoxy groups and F1 atom. Also, a negative electrostatic potential region is observed around the N1 atom. The negative V(r) values are −0.062 a.u. for O1 atom, which is the most negative region: about −0.031 and −0.041 a.u. for O2 and O3 atoms, respectively, −0.030 a.u. for F1 atom and −0.027 a.u. for N1 atom, which is the least negative region. However, maximum positive regions are localized on the hydrogen atom of methoxy groups, which can be considered as possible sites for nucleophilic attack, with a maximum value of 0.054 a.u. According to these calculated results, the MEP map shows that the negative potential sites are on electronegative atoms as well as the positive potential sites are around the hydrogen atoms. These sites give information about the region from where the compound can have noncovalent interactions.

What happens to the electrostatic potential when an intramolecular interaction is taking place is that the potential of the negative atom becomes less negative and the positive region on the other atom becomes less positive [64–66]. So that the lack of a negative region near the nitrogen involved in the hydrogen bond N1···H1-O1, and also the lack of a strong positive region by the involved hydrogen, is indicative of an intramolecular interaction.

Natural bond orbital (NBO) analysis

Selected NBO occupancies at bond critical points for the title compound are listed in Table 5, which were calculated on the B3LYP/6–31G(d) optimized structure.

NBO analyses reveal that the N1=C7 bond has the character of double bond, which is evident by B3LYP method. In flourophenyl and dimethoxyphenyl rings, the C-C bonds are typical single-double arrangement, which form the conjugate structure. The NBO occupancies of F1-C11 bond are larger than those of O2–C2 and O3–C4 bonds, indicating that the strength of bond F1–C11 is stronger than that of O2–C2 and O3–C4 bonds. All the results predicted here are consistent with the information obtained from the bond distances of the crystal structure.

In addition, intra and intermolecular interaction of the stabilization energies of the title compound were performed by using second order perturbation theory and listed in Table 6. For each donor NBO(i) and acceptor NBO(j), the stabilization energy $E^{(2)}$ associated with electron delocalization between donor and acceptor is estimated as [67, 68]

$$E^{(2)} = -q_i \frac{(F_{ij})^2}{\varepsilon_j - \varepsilon_i} \tag{2}$$

where q_i is the donor orbital occupancy, ε_i, ε_j are diagonal elements (orbital energies), and F_{ij} is the off-diagonal NBO Fock matrix element.

The n(N1)→σ(O1-H1) interactions give the strongest stabilization to the system of the title compound by 34.83 kcal mol^{-1} and strengthens the intramolecular O1-H1···N1 hydrogen bond. The lone pairs of F1 donates its

Table 7 Thermodynamic properties at different temperatures at B3LYP/6–31G(d) level

T (K)	$H_m^0\,(kcal.mol^{-1})$	$C_{p,m}^0\,(cal.mol^{-1}.K^{-1})$	$S_m^0\,(cal.mol^{-1}.K^{-1})$
200	5.98	49.75	115.34
250	8.83	60.31	128.02
298.15	12.07	70.35	139.86
300	12.20	70.73	140.31
350	16.09	80.76	152.28
400	20.47	90.15	163.95
450	25.29	98.77	175.31
500	30.53	106.57	186.30

electrons to the σ-type antibonding orbital for C3-H3. The total stabilization energy of C3-H3···F1 intermolecular hydrogen bonding is 1.96 kcal mol^{-1}. There is another NBO interaction of the n(O1)→σ(C5-H5) imply the existence of C5-H5···O1 hydrogen bond which has the total stabilization energy 1.49 kcal mol^{-1}. Thus, it is apparent that C-H···O and C-H···F intermolecular interactions significantly influence crystal packing in this molecule.

Thermodynamic properties

On the basis of vibrational analysis and statistical thermodynamics, the standard thermodynamic functions: heat capacity ($C^0_{p,m}$), entropy (S^0_m), and enthalpy (H^0_m) were obtained at B3LYP/6–31G(d) level and listed in Table 7. Table 7 shows that the standard heat capacities, entropies, and enthalpies increase at any temperature from 200.00 to 500.00 K, because the intensities of molecular vibration increase with the increasing temperature.

The correlation equations between these thermodynamic properties and temperature T are as follows:

$$C^0_{p,m} = 0.13857 + 0.26961\mathrm{T} - 1.12759\mathrm{T}^2 \times 10^{-4} \; ; \left(\mathrm{R}^2 = 0.99988\right) \quad (3)$$

$$S^0_m = 61.55492 + 0.28203\mathrm{T} - 6.50527\mathrm{T}^2 \times 10^{-5}; \left(\mathrm{R}^2 = 1\right) \quad (4)$$

$$H^0_m = -0.83722 + 0.0147\,\mathrm{T} + 9.62365\,\mathrm{T}^2 \times 10^{-5}; \left(\mathrm{R}^2 = 0.99998\right) \quad (5)$$

These equations will be helpful for further studies of the title compound.

Conclusions

2-[(4-Fluorophenylimino)methyl]-3,5-dimethoxyphenol has been synthesized and characterized by IR, UV-Vis, and X-ray single-crystal diffraction. The comparisons between the calculated results and the X-ray experimental data indicate that B3LYP method is better than HF method in evaluating bond lengths and angles. However, the HF method seems to be more appropriate than B3LYP method for obtaining the 3-D geometry of the title compound. For the calculation of vibrational frequencies both the methods B3LYP and HF can predict the IR spectrum of title compound well. The TD-DFT calculations lead to a very close agreement with the experimental absorption spectra both gas phase and solvent media. Molecular orbital coefficients analyses suggest that the electronic spectra is corresponding to $\pi\rightarrow\pi^*$ electronic transition. The MEP map shows that the negative potential sites are on electronegative atoms as well as the positive potential sites are around the hydrogen atoms. These sites give information about the region from where the compound can have noncovalent interactions. The correlations between the thermodynamic properties $C^o_{p,m}$, S^o_m , H^o_m and temperatures T are also obtained.

Acknowledgments This study was supported financially by the Research Centre of Ondokuz Mayis University (Project No: F-476).

References

1. Barton D, Ollis WD (1979) Comprehensive Organic Chemistry, vol 2. Pergamon, Oxford
2. Layer RW (1963) Chem Rev 63:489–510
3. Ingold CK (1969) Structure and Mechanism in Organic Chemistry, 2nd edn. Cornell Univ, Ithaca
4. Taggi AE, Hafez AM, Wack H, Young B, Ferraris D, Lectka T (2002) J Am Chem Soc 124:6626–6635
5. Novopoltseva OM (1995) Cand Sci (Chem). Dissertation, Volgograd
6. Cohen MD, Schmidt GMJ, Flavian S (1964) J Chem Soc 2041–2051
7. Hadjoudis E, Vitterakis M, Mavridis IM (1987) Tetrahedron 43:1345–1360
8. Xu XX, You XZ, Sun ZF, Wang X, Liu HX (1994) Acta Crystallogr A C50:1169–1171
9. Alarcon SH, Pagani D, Bacigalupo J, Olivieri AC (1999) J Mol Struct 475:233–240
10. Köysal Y, Işık Ş, Ağar E (2007) Acta Crystallogr E63:o4916
11. Özek A, Büyükgüngör O, Albayrak Ç, Odabaşoğlu M (2009) Acta Crystallogr E65:o791
12. Kılıç I, Ağar E, Erşahin F, Işık Ş (2009) Acta Crystallogr E65: o934
13. Temel E, Albayrak Ç, Odabaşoğlu M, Büyükgüngör O (2007) Acta Crystallogr E63:o374–376
14. Özek A, Albayrak Ç, Odabaşoğlu M, Büyükgüngör O (2007) Acta Crystallogr C63:o177–o180
15. Karabıyık H, Ocak İskeleli N, Petek H, Albayrak Ç, Ağar E (2008) J Mol Struct 873:130–136
16. Koşar B, Büyükgüngör O, Albayrak Ç, Odabaşoğlu M (2004) Acta Crystallogr C60:o458–o460
17. Tanak H, Erşahin F, Ağar E, Büyükgüngör O, Yavuz M (2008) Anal Sci 24:237–238
18. Zhang Y, Guo ZJ, You XZ (2001) J Am Chem Soc 123:9378–9387
19. Proft FD, Geerlings P (2001) Chem Rev 101:1451–1464
20. Fitzgerald G, Andzelm J (1991) J Phys Chem 95:10531–10534
21. Ziegler T (1991) Pure Appl Chem 63:873–878
22. Andzelm J, Wimmer E (1992) J Chem Phys 96:1280–1303
23. Scuseria GE (1992) J Chem Phys 97:7528–7530
24. Dickson RM, Becke AD (1993) J Chem Phys 99:3898–3905
25. Johnson BG, Gill PMW, Pople JA (1993) J Chem Phys 98:5612–5626
26. Jian FF, Zhao PS, Bai ZS, Zhang L (2005) Struct Chem 16:635–639
27. Schlegel HB (1982) J Comput Chem 3:214–218
28. Peng C, Ayala PY, Schlegel HB, Frisch MJ (1996) J Comput Chem 17:49–56

29. Frisch MJ, Trucks GW, Schlegel HB, Scuseria GE, Robb MA, Cheeseman JR, Montgomery JA Jr, Vreven T, Kudin KN, Burant JC, Millam JM, Iyengar SS, Tomasi J, Barone V, Mennucci B, Cossi M, Scalmani G, Rega N, Petersson GA, Nakatsuji H, Hada M, Ehara M, Toyota K, Fukuda R, Hasegawa J, Ishida M, Nakajima T, Honda Y, Kitao O, Nakai H, Klene M, Li X, Knox JE, Hratchian HP, Cross JB, Bakken V, Adamo C, Jaramillo J, Gomperts R, Stratmann RE, Yazyev O, Austin AJ, Cammi R, Pomelli C, Ochterski JW, Ayala PY, Morokuma K, Voth GA, Salvador P, Dannenberg JJ, Zakrzewski VG, Dapprich S, Daniels AD, Strain MC, Farkas O, Malick DK, Rabuck AD, Raghavachari K, Foresman JB, Ortiz JV, Cui Q, Baboul AG, Clifford S, Cioslowski J, Stefanov BB, Liu G, Liashenko A, Piskorz P, Komaromi I, Martin RL, Fox DJ, Keith T, Al-Laham MA, Peng CY, Nanayakkara A, Challacombe M, Gill PMW, Johnson B, Chen W, Wong MW, Gonzalez C, Pople JA (2004) Gaussian 03, Revision E.01. Gaussian Inc, Wallingford
30. Foresman JB, Frisch A (1996) Exploring chemistry with electronic structure methods, 2nd edn. Gaussian Inc, Pittsburgh
31. Frisch A, Dennington R II, Keith T, Millam J, Nielsen AB, Holder AJ, Hiscocks J (2007) GaussView Reference, Version 4.0. Gaussian Inc, Pittsburgh
32. Miertus S, Scrocco E, Tomasi J (1981) Chem Phys 55:117–129
33. Barone V, Cossi M (1998) J Phys Chem A 102:1995–2001
34. Cossi M, Rega N, Scalmani G, Barone V (2003) J Comput Chem 24:669–681
35. Tomasi J, Mennucci B, Cammi R (2005) Chem Rev 105:2999–3094
36. Runge E, Gross EKU (1984) Phys Rev Lett 52:997–1000
37. Stratmann RE, Scuseria GE, Frisch MJ (1998) J Chem Phys 109:8218–8224
38. Bauernschmitt R, Ahlrichs R (1996) Chem Phys Lett 256:454–464
39. Casida ME, Jamorski C, Casida KC, Salahub DR (1998) J Chem Phys 108:4439–4449
40. Politzer P, Murray J (2002) Theor Chem Acc 108:134–142
41. Moustakali-Mavridis I, Hadjoudis E, Mavridis A (1978) Acta Crystallogr B34:3709–3715
42. Bernstein J, Davies RE, Shimoni L, Chang NL (1995) Angew Chem Int Ed Engl 34:1555–1573
43. Teimouri A, Emami M, Chermahini AN, Dabbagh HA (2009) Spectrochim Acta Part A 71:1749–1755
44. Yeap GY, Ha ST, Ishizawa N, Suda K, Boey PL, Mahmood WAK (2003) J Mol Struct 658:87–99
45. Ünver H, Yildiz M, Kiraz A, Özgen Ö (2009) J Chem Crystallogr 39:17–23
46. Abkowicz-Bienko AJ, Bienko DC, Latajka Z (2000) J Mol Struct 552:165–175
47. Masternak A, Wenska G, Milecki J, Skalski B, Franzen S (2005) J Phys Chem 109:759–766
48. Le Y, Chen JF, Pu M (2008) Int J Pharm 358:214–218
49. Ledbetter JW Jr (1968) J Phys Chem 72:4111–4115
50. Dudek GO, Dudek EP (1966) J Am Chem Soc 88:2407–2412
51. Salman SR, Shawkat SH, Al-Obaidi GM (1989) Spectrosc Lett 22:1265–1273
52. Yıldız M, Kılıç Z, Hökelek T (1998) J Mol Struct 441:1–10
53. Nazır H, Yıldız M, Yılmaz H, Tahir MN, Ülkü D (2000) J Mol Struct 524:241–250
54. Ünver H, Yıldız M, Zengin DM, Özbey S, Kendi E (2001) J Chem Crystallogr 31:211–216
55. Salman SR, Kamounah FS (2002) Spectrosc Lett 35:327–335
56. Yıldız M (2004) Spectrosc Lett 37:367–381
57. Dziembowska T, Jogodzinska E, Rozwadowski Z, Kotfica M (2001) J Mol Struct 598:229–234
58. Rong ZC, Jiang LZ, Hong CY, Shan CH, Zhi Wu Y, Hua YL (2009) THEOCHEM 899:86–93
59. Scrocco E, Tomasi J (1978) Adv Quantum Chem 11:115–121
60. Luque FJ, Lopez JM, Orozco M (2000) Theor Chem Acc 103:343–345
61. Politzer P, Laurence PR, Jayasuriya K, McKinney J (1985) Special issue of Environ Health Perspect 61:191–202
62. Scrocco E, Tomasi J (1973) Topics in Current Chemistry, vol. 7. Springer Verlag, Berlin, p 95
63. Politzer P, Truhlar DG (1981) Chemical Applications of Atomic and Molecular Electrostatic Potentials. Plenum, New York
64. Hussein W, Walker CG, Peralta-Inga Z, Murray JS (2001) Int J Quantum Chem 82:160–169
65. Politzer P, Concha MC, Murray JS (2000) Int J Quantum Chem 80:184–192
66. Özdemir N, Dinçer M, Çukurovalı A (2009) J Mol Model. doi:10.1007/s00894-009-0552-8
67. Schwenke DW, Truhlar DG (1985) J Chem Phys 82:2418–2427
68. Gutowski M, Chalasinski G (1993) J Chem Phys 98:4728–4738